J. Fluid Mech. (2003), *vol.* 481, *pp.* 355–384.
DOI: 10.1017/S0022112003004087 Printed in the United Kingdom

Confined turbulent convection

By J. J. NIEMELA[1] AND K. R. SREENIVASAN[2]

[1] Cryogenic Helium Turbulence Laboratory, Department of Physics, University of Oregon, OR 97403, USA

[2] Institute for Physical Science and Technology, University of Maryland, College Park, MD 20742, USA

(Received 3 June 2002 and in revised form 19 December 2002)

New measurements of the Nusselt number have been made in turbulent thermal convection confined in a cylindrical container of aspect ratio unity. The apparatus is essentially the same as that used by Niemela *et al.* (2000), except that the height was halved. The measurement techniques were also identical but the mean temperature of the flow was held fixed for all Rayleigh numbers. The highest Rayleigh number was 2×10^{15}. Together with existing data, the new measurements are analysed with the purpose of understanding the relation between the Nusselt number and the Rayleigh number, when the latter is large. In particular, the roles played by Prandtl number, aspect ratio, mean wind, boundary layers, sidewalls, and non-Boussinesq effects are discussed. Nusselt numbers, measured at the highest Rayleigh numbers for which Boussinesq conditions hold and sidewall forcing is negligible, are shown to vary approximately as a 1/3-power of the Rayleigh number. Much of the complexity in interpreting experimental data appears to arise from aspects of the mean flow, including complex coupling of its dynamics to sidewall boundary conditions of the container. Despite the obvious practical difficulties, we conclude that the next generation of experiments will be considerably more useful if they focus on large aspect ratios.

1. Introduction

A major item of interest in thermal convection is the heat transport across a horizontal layer of fluid confined between two parallel plates when the bottom plate is maintained sufficiently hotter than the top that the resulting flow is turbulent. This problem is posed in terms of the dependence of the Nusselt number, Nu, on the Rayleigh number, Ra, and the Prandtl number, Pr. Here, Nu is the ratio of the measured total heat flux to that due entirely to molecular conduction. The Rayleigh number is the non-dimensional measure of the prescribed temperature difference, and is given by $Ra \equiv \alpha \Delta T g H^3/\nu\kappa$, where α is the isobaric thermal expansion coefficient of the fluid in the container, ΔT is the temperature difference between the bottom and top walls, g the acceleration due to gravity, H the vertical dimension of the convection cell; ν and κ are, respectively, the kinematic viscosity and the thermal diffusivity of the fluid, and $Pr = \nu/\kappa$. Of particular interest is the relation between Nu and Ra when the latter is large. The interest arises not only because of the intrinsic importance of the asymptotic state of thermal convection but also because one encounters very large values of Ra in geophysical and astrophysical contexts (see, for example, Sreenivasan & Donnelly 2001 for a discussion of the typical values of Ra).

Thus, there has been a push to attain high Rayleigh numbers in controlled laboratory experiments (e.g. Castaing *et al.* 1989; Chavanne *et al.* 1997; Niemela *et al.* 2000). In particular, the experiments of Niemela *et al.* (2000) (which will be referred to as I henceforth) spanned 11 decades of Ra and reached 10^{17}. Despite this and other significant efforts there are several unresolved questions relating to the scaling properties of heat transport in the high-Ra range. The reason is partly that the laboratory experiments have been in containers with the aspect ratio Γ, defined here as the ratio of the horizontal dimension of the container to its vertical dimension, of the order unity. The vertical dimension must be large to attain large values of Ra and it is not always practical to scale up the horizontal dimension as well. Thus, Γ becomes an additional parameter in the problem. Other 'practical' problems are that the Prandtl number in some recent experiments was not held fixed at the high end of the Rayleigh number range, and it has been difficult to stay within the small bounds of the so-called Boussinesq approximation when Ra values are large. Both problems come into play simultaneously as the pressure or density of a heated gas layer is pushed closer towards the critical values.

To understand these effects, we have made new measurements in a container of aspect ratio unity and analysed the experimental conditions in several previously published data. This work sheds new light on the subject, making moot a few previous directions of enquiry; however, it raises additional questions that need to be addressed. We interpret our findings in terms of existing theories about turbulent convection, making comparisons with available data wherever possible. A qualitative conclusion is that the constraint of small aspect ratio has important effects on the state of convection, even at very high Ra, and that care should be exercised in comparing existing data with theories that invoke infinite horizontal extent of the flow. The inference is thus almost tautological that experiments at larger aspect ratio and high Rayleigh numbers would have to be the next focus.

Section 2 highlights an unresolved puzzle in a way that naturally paves the way for new experiments. The description of the experimental apparatus in § 3 is followed in § 4 by a brief presentation of the new Nusselt number data. Section 5 considers heat transport at intermediate Rayleigh numbers, and is followed by § 6 devoted to heat transport at high Rayleigh numbers under Boussinesq conditions. The boundary layer structure under possibly non-Boussinesq conditions is discussed in § 7, and concluding remarks are presented in § 8. The appendices summarize important aspects secondary to the main thread of the paper.

2. An unresolved puzzle

An unsolved puzzle in turbulent convection is illustrated in figure 1 where we have plotted Nu against Ra from I and Chavanne *et al.* (2001), which we shall henceforth refer to as II. For the present discussion, only a part of the Ra range covered in I and II is shown. Note that the data from II differ somewhat from those tabulated in Chavanne (1997) (see also Chavanne *et al.* 1997) because of an adjustment to the 1990 International Temperature Scale. This adjustment, though quantitatively significant for $Ra > 10^{11}$, does not make any difference to the qualitative conclusions to be drawn.

There are conspicuous differences between the two sets of data, both in the magnitude and the rate of increase of the heat transfer with Ra. This latter aspect is further illustrated in the inset. Here, it can be seen that the exponent β in the presumed power-law relation $Nu = mRa^{\beta}$ varies little, by comparison, over the entire

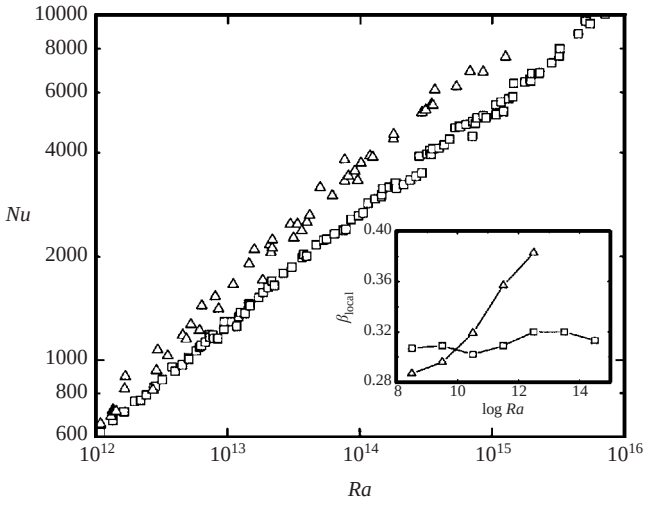

FIGURE 1. The variation of the Nusselt number with the Rayleigh number in log–log coordinates, from I (□) and II (△), illustrating the difference for $Ra > 10^{12}$. Inset shows approximate local slopes, $\beta_{local} = \mathrm{d}\log(Nu)/\mathrm{d}\log(Ra)$, obtained by least squares fits over running intervals of three decades. Various trials suggest that local slopes are less robust if shorter running intervals are used.

range of I, with an average value of about 0.31. In contrast, in II the slope increases sharply for higher *Ra*, approaching its maximum value of nearly 0.4 at $Ra \sim 10^{12}$, so this behaviour has been regarded as being consistent with Kraichnan's (1962) prediction of $Ra^{1/2}/[(\ln Ra)^{3/2}]$. It is important to point out, however, that the slopes are necessarily averages computed over 3-decade intervals of *Ra* (see caption to figure 1) and hence are only approximate indications of the local behaviour. For the same reason, they cannot address the behavior at the highest *Ra*, which we will consider more appropriately below (see § 6.2).

Both sets of data were obtained in cylindrical containers of aspect ratio 1/2. In addition, several discussions among the participants in these two experimental programs have indicated that minor differences in the apparatus and measurement methods cannot explain the differences; this point will be put on a considerably firmer foundation by the new data to be presented in § 4. It is legitimate to ask if the observed differences are due to differences in *Pr* values, particularly since the aspect ratio is the same for the two experiments. In principle, the flow depends on both *Ra* and *Pr* and, as mentioned in § 1, *Pr* in both experiments varies simultaneously with *Ra* when *Ra* is high.

This question may be discussed in terms of the *Ra*–*Pr* phase diagram proposed by Grossmann & Lohse (2000, 2001, 2002). From considerations of the energy and temperature dissipation rates in boundary layers and the bulk, these authors isolated possible states of convection; the essential aspects of their results are reproduced in figure 2. These authors noted that, while each region would in principle exhibit unique scaling relations between *Nu* and *Ra*, the influence from other regions would in practice influence the power laws, this influence being more or less dependint on the distance to neighbouring regions. The two sets of data from I and II are plotted in figure 2. Except at low Rayleigh numbers, both sets of data are within region $\mathrm{IV_u}$, suggesting the possibility that they should possess the same behavior. That this does not happen suggests the presence of additional aspects of the problem. One such

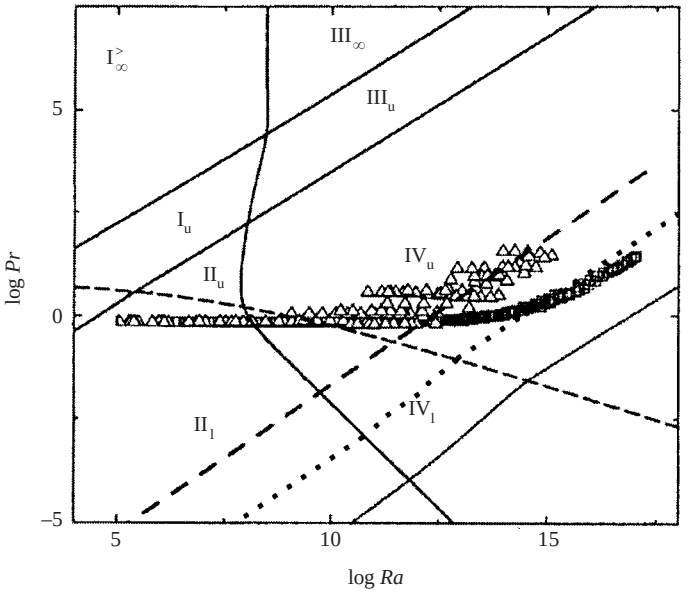

FIGURE 2. The data from I (□) and II (△) are plotted in the phase diagram of Grossmann & Lohse in the (*Ra*, *Pr*)-plane. Marked by Roman numerals are regions of different characteristic power laws, although neighbouring regions can have some influence on the observed power laws, depending on the nearness to boundaries. In particular, data that span more than one region are not expected to have a pure power law, but combinations of them. The thick long-dashed line denotes the minimum *Ra* for which the velocity boundary layers are likely to be turbulent (see Appendix A). The dotted line just to the right of it results from a new calculation by Grossmann & Lohse (2002) for the onset of turbulence in the velocity boundary layer. It replaces their earlier boundary (Grossmann & Lohse 2001) shown farthest to the right as the full line. While these boundaries are not sharp, their location has some bearing on the interpretation of differences between the two data sets shown.

aspect is the transition of the velocity boundary layer from laminar to the turbulent state. The long-dashed line in figure 2, given by (A 3) in Appendix A (see also § 7), denotes a rough approximation to the minimum *Ra* below which the velocity boundary layers does not remain turbulent. A recent theory of Grossmann & Lohse (2002) (see also their 2000 paper) gives another plausible boundary for the transition between the laminar and turbulent states; this is shown by the dotted line in figure 2. The relevance of this boundary to the observed heat transfer depends, among other factors, on the relative thicknesses of the thermal and viscous boundary layers, as will be discussed in § 7.

3. Some experimental details of the new measurements

Selective repeats of the measurements of I only served to confirm them, so we altered the convection apparatus in the simplest possible manner to allow new measurements and focus attention on flow physics. The apparatus, cylindrical in shape, was the same as in I except that its height was halved from 100 cm to 50 cm (new $\Gamma = 1$). The top and bottom plates, 3.8 cm in thickness, were made of copper annealed under oxygen-free conditions; its thermal conductivity at a temperature of 5 K was a relatively high value of order $2\,\mathrm{kW\,m^{-1}\,K^{-1}}$. Special efforts were made to heat the plates uniformly. A constant heat flux occurred at the bottom plate

whenever experimental conditions were altered, but measurements were begun only after a constant temperature was reached in the steady state. The top wall was connected to a helium reservoir through a distributed and adjustable thermal link, and its temperature was maintained constant by means of a resistance bridge and servo. The stainless steel sidewall had a thickness of 0.267 cm. The inner convection cell was insulated by three thermal shields at various graded temperatures, residing in a common vacuum space. Due to the relatively large height of the apparatus, corrections were made for the small adiabatic temperature gradient across the fluid layer (see Tritton 1988, appendix to chapter 14).

For a subset of measurements, a further modification of the apparatus was made by adding an insulating layer of polyethylene terephthalate (Mylar) to the entire inner surface of the sidewall. One purpose of adding the insulation, motivated by discussions in Ahlers (2001) and Roche *et al.* (2001), was to reduce the lateral heat currents near the horizontal boundaries through the addition of an extra thermal impedance (an effect nominally estimated to require a correction of a few percent to Nu at moderately low Rayleigh numbers). Specifically, the Mylar strip had a thickness of 0.127 mm overall, but the flange region just above the bottom plate and also below the top plate, connecting these plates to the sidewall, was covered with an additional 2.5 cm wide strip of the same Mylar sheet. A thin layer of low-viscosity Stycast 1266 epoxy was used to bond the Mylar sheets to the sidewall. From Childs, Ericks & Powell (1973), we estimate the conductivity of Mylar to be approximately between 0.0015 and 0.002 W m^{-1} K^{-1} at a temperature of 5 K (using a linear extrapolation from 28 K in log–log coordinates of thermal conductivity and temperature). The conductivity of Type 304 stainless steel at the same temperature (see Jensen *et al.* 1980) is approximately 0.25 W m^{-1} K^{-1}. The sidewall resistance is thus judged to have increased by roughly an order of magnitude, for moderate Ra, with respect to lateral conduction between the fluid and the sidewall.

For the new data, the mean cell temperature was kept within the limits $T_M = 5.34 \pm 0.02$ K. Holding the mean temperature fixed has the advantage that the variation of fluid properties occurs through pressure dependence alone. In practice, this increases the precision with which Nu and Ra can be determined. This increased precision is manifested as reduced scatter in subsequent figures. The data, especially at high Ra, were not all taken in a chronological sequence; that is, no particular history was imposed on the system and no hysteresis was observed. All quantities are evaluated using fluid properties at the mean temperature. (In low-Rayleigh-number convection, this practice ensures that measures of non-Boussinesqness remain small even if there are small deviations from vertical symmetry about the mid-plane; see Busse 1967. For our conditions, it is merely the most logical thing to do.) The critical temperature and density, corresponding to the temperature scale used (1990 International Temperature Scale) are, respectively, $T_C = 5.195$ K, and $\rho_C = 69.64$ kg m^{-3}.

The Nusselt numbers were calculated by subtracting the parallel 'empty cell' sidewall conduction. This 'correction' is now known to be in principle inadequate because the temperature gradients in the sidewalls are much sharper where they connect to the bottom and top plates (Ahlers 2001; Roche *et al.* 2001, appendix B) when the enclosed fluid has a thin thermal boundary layer structure (i.e. under conditions of high imposed heat flux). In fact, an additional adjustment appears necessary for $Ra \lesssim 10^{11}$ if our interest lies in Nusselt numbers for the ideal case of adiabatic sidewalls (see, particularly, the recent numerical results of Verzicco 2002, for $\Gamma = 1/2$). While we discuss this problem at some length below and in Appendix B, we

have not attempted to make these corrections explicitly: a quantitatively precise magnitude of this correction is still difficult to determine, and even a complete qualitative understanding seems elusive, at least for general Γ. We point out, however, that our interest is in the high-Rayleigh-number range, where this type of correction becomes diminishingly small. No corrections have been applied to any data among which we make comparisons throughout, these having been obtained in cryogenic apparatus very similar to ours in terms of sidewall effects (Roche *et al.* 2002).

The heat leaked from the bottom plate into the sidewall has various effects. Some of that heat returns to the fluid very near the bottom of the sidewall through conduction, participates in the convection process within the apparatus, and escapes again by conduction into the sidewall near the top of the sidewall, finally escaping into the top plate. To the extent that this heat participates in convection, one may be tempted to think that this is not a major concern. On the other hand, if one looks only at the global balance just at the level of the bottom and top plates, and ignores what happens in between, it appears that a correction will indeed be needed. In fact, the Nusselt numbers which take account of only the 'empty-cell' correction are found to be reasonably close to the exact *Nu* calculated from turbulent heat flux for the confined system (Verzicco 2002), even though the details of the heat current in the walls are quite complicated. The main effect of the sidewall conduction, deduced from the numerical simulations of Verzicco (2002), is the forcing it provides to the mean flow by the lateral component of the heat current. This effect, obviously absent in the ideal case, cannot be parameterized readily; in particular, it would *a priori* seem that the forcing would depend sensitively on small details of boundary conditions. Moreover, this might be expected to be sensitive to the aspect ratio, since, for example, the mean flow structure exhibits qualitative and measurable differences between $\Gamma = 1/2$ and $\Gamma = 1$ (Verzicco & Camussi 1999, 2003; Qui & Tong 2001). An argument could be made that the mean flow that is characteristic of aspect ratio unity, consisting of a single roll embedded within the entire apparatus, would be subject to either enhanced or depleted buoyancy from sidewall currents. This has already been proposed by Sreenivasan, Bershadskii & Niemela (2002) as an explanation for the occurrence of occasional and non-periodic reversals of the mean flow direction.

4. New data on the Nusselt number

Figure 3 compares the new Nusselt numbers with those from I and II. (Table 1 presents a useful list of experimental parameters, some of which are considered in later sections.) The similarities are obvious, but the new data differ in detail from those of both I and II. In particular, consistent with the thinking of Grossmann & Lohse (2000), it is clear that a single power law is inadequate to describe the heat transfer scaling in the new data over the entire range of *Ra*, even though, to the lowest order, such a fit holds good for the case $\Gamma = 1/2$. A resolution of the differences should contribute to a fuller understanding of the high-*Ra* convection. This is our major goal here. We emphasize that the bottom and top plates, as well as the entire thermal control and measurement system, were identical in the present experiments and I. This fact, as we shall see more clearly below, negates the likelihood that some unknown detail in boundary conditions or measurement procedure may explain the puzzle introduced in § 2.

A more refined comparison of differences among the three experiments is made in figure 4, where we plot *Nu* compensated by $Ra^{0.309}$. The exponent of 0.309 comes from

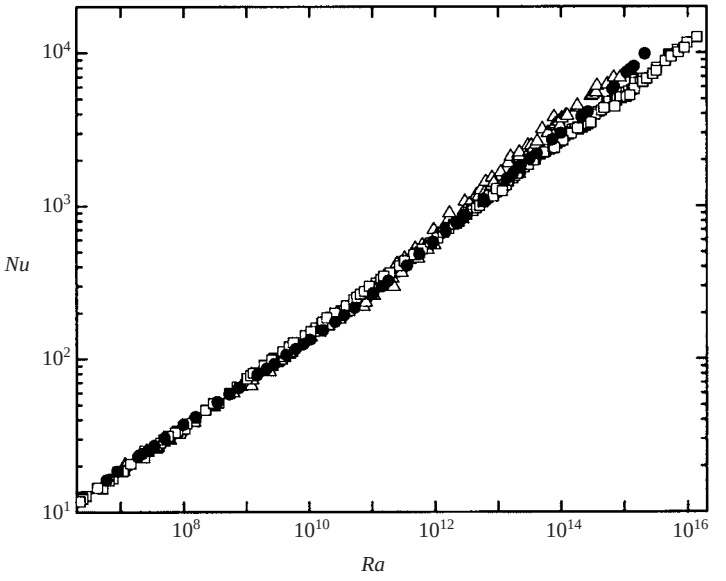

FIGURE 3. The variation of Nusselt number with Rayleigh number in log–log coordinates, from I (□) and II (△), compared with the present data (●). Only data determined to be 'nominally' Boussinesq by the various authors are shown. For all sets of data, this nominal criterion corresponds roughly to $\alpha\Delta T < 0.2$. We shall examine the adequacy of this criterion in § 6.1 and Appendix C.

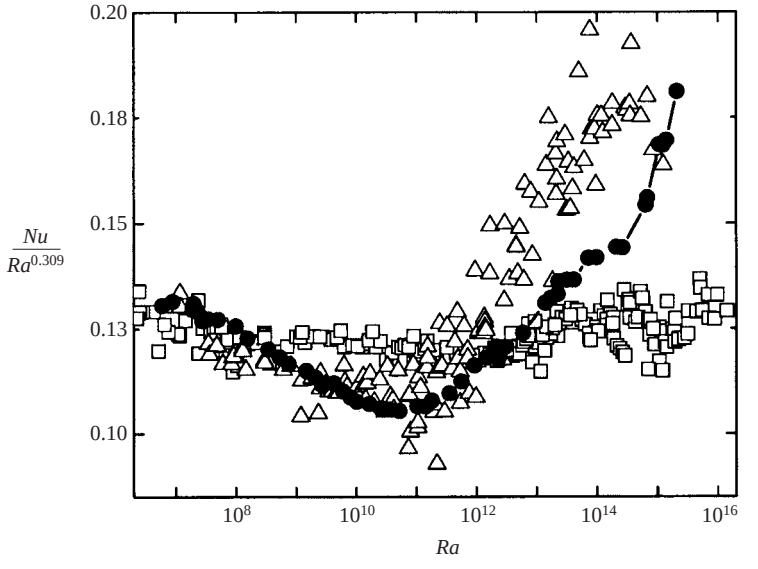

FIGURE 4. The Nusselt number data normalized by the 0.309 power of *Ra* for the same data as in figure 3. The present data (●) are similar to II (△) for low *Ra* but fall roughly intermediate between I (□) and II for high *Ra*. As in figure 3, only the data for which nominal Boussinesq conditions hold have been plotted.

I for aspect ratio 1/2 where it represents a lowest-order fit over the entire range of *Ra*, and is used here for nominal comparisons only. In relation to I, the data from II lie slightly above for low *Ra*, go below for an intermediate range of *Ra*, and rise

Q (mW)	ΔT (mK)	T_M (K)	ρ (kg m^{-3})	ν (m^2 s^{-1})	Ra	Nu	Pr	$\alpha\Delta T$
11.4	171	5.39	0.0201	6.63×10^{-5}	5.97×10^{6}	16.2	0.68	0.032
20.1	264	5.43	0.0200	6.74×10^{-5}	8.86×10^{6}	18.4	0.68	0.049
20.1	214	5.41	0.0321	4.17×10^{-5}	1.88×10^{7}	22.9	0.68	0.040
11.4	119	5.36	0.0436	3.05×10^{-5}	1.98×10^{7}	23.6	0.68	0.022
11.4	117	5.36	0.0463	2.87×10^{-5}	2.19×10^{7}	24.0	0.68	0.022
5.06	50.4	5.33	0.0788	1.68×10^{-5}	2.75×10^{7}	25.3	0.68	0.010
20.1	183	5.40	0.0465	2.87×10^{-5}	3.40×10^{7}	27.1	0.68	0.034
11.4	93	5.35	0.0784	1.69×10^{-5}	5.03×10^{7}	30.5	0.68	0.018
11.4	76.8	5.34	0.121	1.09×10^{-5}	9.93×10^{7}	37.2	0.68	0.015
20.1	120	5.36	0.122	1.09×10^{-5}	1.56×10^{8}	41.7	0.68	0.023
11.4	55.2	5.33	0.265	4.99×10^{-6}	3.45×10^{8}	52.2	0.68	0.011
20.1	86	5.34	0.265	5.02×10^{-6}	5.34×10^{8}	58.8	0.68	0.016
31.4	122	5.36	0.266	5.01×10^{-6}	7.58×10^{8}	64.6	0.68	0.023
20.1	64.9	5.33	0.505	2.63×10^{-6}	1.48×10^{9}	78.5	0.69	0.012
31.4	92	5.35	0.504	2.64×10^{-6}	2.09×10^{9}	86.0	0.69	0.018
45.2	122	5.36	0.507	2.63×10^{-6}	2.79×10^{9}	92.6	0.69	0.023
20.2	48.3	5.32	0.987	1.35×10^{-6}	4.30×10^{9}	106	0.69	0.009
31.5	68.5	5.33	0.985	1.36×10^{-6}	6.08×10^{9}	116	0.69	0.013
45.2	91	5.35	0.986	1.36×10^{-6}	8.06×10^{9}	125	0.69	0.018
61.6	116	5.36	0.988	1.36×10^{-6}	1.02×10^{10}	133	0.69	0.022
45.2	74	5.34	1.55	8.66×10^{-7}	1.66×10^{10}	154	0.70	0.015
80.8	116	5.36	1.55	8.69×10^{-7}	2.58×10^{10}	175	0.70	0.023
61.4	79.9	5.34	2.16	6.24×10^{-7}	3.59×10^{10}	193	0.71	0.016
102	118	5.36	2.16	6.26×10^{-7}	5.24×10^{10}	216	0.71	0.024
80.7	74.7	5.34	3.69	3.71×10^{-7}	1.04×10^{11}	270	0.74	0.016
126	105	5.35	3.69	3.72×10^{-7}	1.44×10^{11}	299	0.74	0.022
102	78	5.34	4.68	2.95×10^{-7}	1.82×10^{11}	325	0.76	0.017
126	76	5.34	6.42	2.18×10^{-7}	3.59×10^{11}	408	0.79	0.018
126	63.9	5.33	8.41	1.69×10^{-7}	5.65×10^{11}	481	0.82	0.016
126	52.4	5.33	11.19	1.30×10^{-7}	9.32×10^{11}	581	0.88	0.015
152	53.3	5.33	13.28	1.12×10^{-7}	1.48×10^{12}	681	0.92	0.017
181	54.5	5.33	15.12	9.95×10^{-8}	2.16×10^{12}	782	0.97	0.018
282	84.9	5.34	13.27	1.12×10^{-7}	2.34×10^{12}	784	0.92	0.026
283	76.2	5.34	15.11	9.98×10^{-8}	3.01×10^{12}	865	0.97	0.026
502	104	5.35	17.26	8.90×10^{-8}	5.98×10^{12}	1100	1.02	0.038
501	71.4	5.34	24.79	6.54×10^{-8}	1.39×10^{13}	1510	1.30	0.038
501	65.2	5.33	26.77	6.14×10^{-8}	1.73×10^{13}	1628	1.40	0.039
722	85.5	5.34	26.74	6.16×10^{-8}	2.24×10^{13}	1776	1.39	0.051
321	35.8	5.32	32.48	5.25×10^{-8}	2.30×10^{13}	1831	1.79	0.030
502	49.8	5.33	32.43	5.26×10^{-8}	3.18×10^{13}	2030	1.78	0.042
722	65.5	5.33	32.4	5.27×10^{-8}	4.14×10^{13}	2202	1.77	0.055
502	34.9	5.32	39.65	4.51×10^{-8}	7.20×10^{13}	2712	2.61	0.048
783	48.7	5.32	39.57	4.52×10^{-8}	9.87×10^{13}	2992	2.58	0.066
783	35.6	5.32	45.69	4.07×10^{-8}	2.10×10^{14}	3843	3.81	0.078
1127	47.2	5.32	45.57	4.08×10^{-8}	2.65×10^{14}	4128	3.72	0.101
1282	35.4	5.32	51.9	3.73×10^{-8}	6.45×10^{14}	5813	5.92	0.130
1489	39.8	5.32	51.79	3.73×10^{-8}	6.85×10^{14}	5990	5.76	0.142
981.7	20.2	5.31	57.73	3.47×10^{-8}	1.08×10^{15}	7446	9.33	0.125
1281	25	5.31	57.41	3.48×10^{-8}	1.23×10^{15}	7756	8.94	0.148
1712	31.5	5.32	57.04	3.50×10^{-8}	1.42×10^{15}	8147	8.53	0.176
1127	16.5	5.31	63.43	3.27×10^{-8}	2.10×10^{15}	9832	13.4	0.155

TABLE 1. Various parameters for the present apparatus, $\Gamma = 1$. Ra and Nu have been corrected for a small adiabatic temperature gradient (approximately 1–2 mK across the cell – see text).

above again at higher *Ra*. The new data for unity aspect ratio display some of the same characteristics of II for low *Ra* but fall roughly between the other two for high *Ra*.

For convenience of further discussion, we loosely subdivide the Rayleigh number range into three parts. At the low end, say $Ra < 10^9$, heat transport is measurably susceptible to details of boundary conditions on the sidewall, and so one has to consider this feature before arriving at firm conclusions. These details are relegated to Appendix B, as already mentioned. In the intermediate range of *Ra* (say $10^9 < Ra < 10^{12}$), the large-scale circulation, resulting from the self-organization of thermal plumes expelled from the top and bottom boundary layers and often called the mean wind (e.g. Castaing *et al.* 1988; Niemela *et al.* 2001*a*; Qiu & Tong 2001; Sreenivasan *et al.* 2002; and Appendix D), seems to play a conspicuous role in convection dynamics; notably, the boundary layers on the bottom and top walls are connected through the wind and the size of the apparatus is thus felt by the convective motion. Beyond Rayleigh numbers of order 10^{12}, the time-averaged mean wind becomes less and less well-defined, and the boundary layers set up by the unsteady large-scale motion are likely to be fully turbulent (see Appendix A). As might be expected, the nature of convection changes as a consequence. This will be designated the high-*Ra* regime.

5. Heat transport in the intermediate-Rayleigh-number regime

Existing estimates suggest that the direct effects of sidewall conduction are reduced to the order of a few percent in this range (see Appendix B). Furthermore, figure 2 shows that the Prandtl numbers from the present experiments and I are constant in this range, though somewhat less so for II. We shall also see in § 6 that the present flow obeys the Boussinesq approximation quite closely, so presumably the Nusselt numbers measured in the region are not affected much by associated artifacts.

It therefore comes as a surprise to us that the agreement among different experiments in this regime is relatively poor, far beyond measurement uncertainties. This can be appreciated from figure 5, in which representative data sets are plotted. We draw several lessons. The open squares and filled circles in the figure are obtained in the same apparatus except for the change of aspect ratio from 1/2 for I to unity for the present data. It is tempting to infer that the differences here are primarily due to the changed aspect ratio. However, the new data for aspect ratio unity are generally in better agreement with the data of II for $\Gamma = 1/2$ (which, because of their relatively larger scatter, are not shown here – but see figure 4). We also show data from Roche (2001), obtained in the same apparatus as II but with systematically roughened walls. Note that this roughness is immaterial here since the walls are 'hydrodynamically smooth' (P. Tong, private communication) at these Rayleigh numbers, i.e. the boundary layers are still thicker than the height of the roughness elements. A subset of Roche's data, open triangles corresponding to $Pr = 0.7$ and open circles corresponding to Pr = 1.5, are in general agreement with the present data ($\Gamma = 1, Pr = 0.7$), while his data for $Pr = 1.1$, shown by filled triangles, agree well with I ($\Gamma = 1/2, Pr = 0.7$). Further, the plusses from Wu (1991) ($\Gamma = 1, Pr = 0.7$) also agree with I ($\Gamma = 1/2, Pr = 0.7$). On the other hand, Wu's data for $\Gamma = 1/2, Pr = 0.7$ agree with the present data ($\Gamma = 1, Pr = 0.7$). Finally, the data from Xu, Bajaj & Ahlers (2000) ($\Gamma = 1/2, Pr = 4$) lie close to, though just above, the present data ($\Gamma = 1, Pr = 0.7$).

In the above discussion, we have provided Prandtl numbers and aspect ratios for each experiment. There does not appear to be any obvious correlation with either.

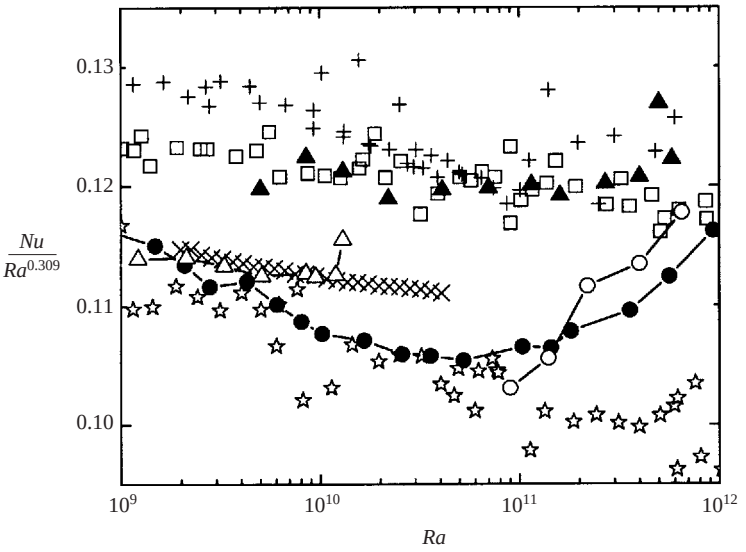

FIGURE 5. Nusselt numbers for the intermediate range of Ra. □, I ($\Gamma = 1/2, Pr = 0.7$); ●, the present data ($\Gamma = 1, Pr = 0.7$); △, Roche (2001) ($\Gamma = 1/2, Pr = 0.7$); ○, Roche (2001) ($\Gamma = 1/2, Pr = 1.5$); ▲, Roche (2001) ($\Gamma = 1/2, Pr = 1.1$); +, Wu (1991) ($\Gamma = 1, Pr = 0.66$); ☆, Wu (1991) ($\Gamma = 1/2, Pr = 0.66$); ×, Xu *et al.* (2000) ($\Gamma = 1/2, Pr = 4$). At least for $Nu < 10^{11}$, the Nu data appear to lie broadly in two bands, uncorrelated with either Γ or Pr.

The prevailing evidence from Ahlers & Xu (2001), Lam *et al.* (2001) and Roche *et al.* (2002) is that the dependence of Nu on the Prandtl number is negligible in the ranges of Ra and Pr considered. The simulations of Kerr (1996) and Kerr & Herring (2000), when taken together, essentially agree with this conclusion. We will return to this issue later, but, assuming for now that Pr matters little, we are led to examine the role of the aspect ratio. While the aspect ratio appears to play some role in determining Nusselt numbers for intermediate Ra (Wu & Libchaber 1991; Niemela *et al.* 2001*b*; Xu *et al.* 2000), it is clear that the differences just listed cannot be simply parameterized by this one factor.

Within this complexity, however, it appears that the data fall roughly within two main bands. This is so even if one restricts attention to the recent high-Ra helium experiments that are nominally similar. This suggests the possible existence of different time-averaged states of the flow for a given set of conditions, which has been recently raised by Roche *et al.* (2002) experimentally, and by Verzicco & Camussi (2003) numerically. Roche *et al.* (2002) conclude that the factor that correlates best with these different states is the mean wind, which itself is determined in some yet unknown way by details such as Pr and geometric parameters of the apparatus (not all of which are represented by the aspect ratio alone). And, even for fixed aspect ratio, the mean wind changes character with Ra. Verzicco & Camussi (2003) observe, for $\Gamma = 1/2$, that the mean wind changes from a weak re-circulation over the entire height of the apparatus, coupled with a stronger but more localized toroidal roll at the top and bottom boundaries at low Ra, to a two-cell structure of equal size, stacked one above the other, and a weaker toroidal roll structure at higher Ra. Such differences seem to arise from delicate interplay among detailed geometry as well as Prandtl and Rayleigh numbers.

From such considerations, we tentatively conclude that the mean wind is a potential candidate for explaining differences among experiments in the intermediate range of *Ra*, without appealing in detail to possible coupling to the sidewall thermal conditions as discussed above. The mean wind has other effects as well – for example, in establishing velocity boundary layers, whose importance we shall examine in § 7. We shall also consider in Appendix E the total energy dissipation as a function of the Reynolds number of the mean wind.

6. High Rayleigh numbers

The questions we wish to address here are: (*a*) What is the nature of the heat transport at the highest Rayleigh numbers measured, for which deviations from the Boussinesq approximation are kept small, say below about 5%? (*b*) When Boussinesq conditions seem to have been seriously violated, what is the qualitative nature of heat transport?

6.1. *The Boussinesq approximation*

In the experiments considered, very high Rayleigh numbers are usually attained by closer approach to the critical point of the gas, and hence are associated with increasingly steep temperature dependences of the various relevant fluid properties. Because the temperatures of the bottom and top plates are maintained ΔT apart, this feature has the effect of producing measurable differences in fluid properties in the bottom and top boundary layers. This vertical asymmetry introduces a variety of additional parameters into the problem. Near the convective onset, for instance, vertical asymmetry can alter the flow structure (Palm 1960; Busse 1978), but less is known about the consequences in the high-*Ra* range.

Figure 6 shows, for the present measurements, the differences between the top and bottom values of specific heat, kinematic viscosity, thermal expansion coefficient, thermal diffusivity, and thermal conductivity of helium gas, as a fraction of their mean values. These fractional deviations are all of the order of 5% or less up to a Rayleigh number of 10^{14}, beyond which a few of them rapidly increase with *Ra* as the critical point of the fluid is approached. Similar deviations occur in I and II.

To ascertain the relevance of these to turbulent convection, we consider the following. In the steady state, the heat transported from the bottom wall to the fluid layer must be transported entirely from the fluid layer to the top wall (ignoring, of course, possible effects of the sidewall). This means that the mean temperature slopes at the two walls have to adjust to the different thermal conductivities of the fluid at the two walls, leading to unequal drops of temperature across the two thermal boundary layers. The ratio of the temperature drops, Δ_C/Δ_H, where Δ_C is the temperature drop across the cold thermal boundary layer and Δ_H that of the hotter boundary, can be estimated from a knowledge of the temperature-dependent fluid properties (Wu & Libchaber 1991), and is plotted for the present data in figure 7. Consistent with the other criteria, Δ_C/Δ_H deviates from unity by less than about 5% up to $Ra \approx 10^{14}$, and increases more rapidly beyond. We make a more detailed examination of non-Boussinesq effects in Appendix C.

These figures suggest that some degree of 'non-Boussinesqness' prevails for $Ra \gtrsim 10^{14}$ in the present experiments. Such effects begin to occur for even lower *Ra* in II and do not appear until higher *Ra* in I. Although none of this necessarily tells us the degree to which non-Boussinesq effects are important in determining the Nusselt number, it is clear that we must exercise caution in comparing data at the highest

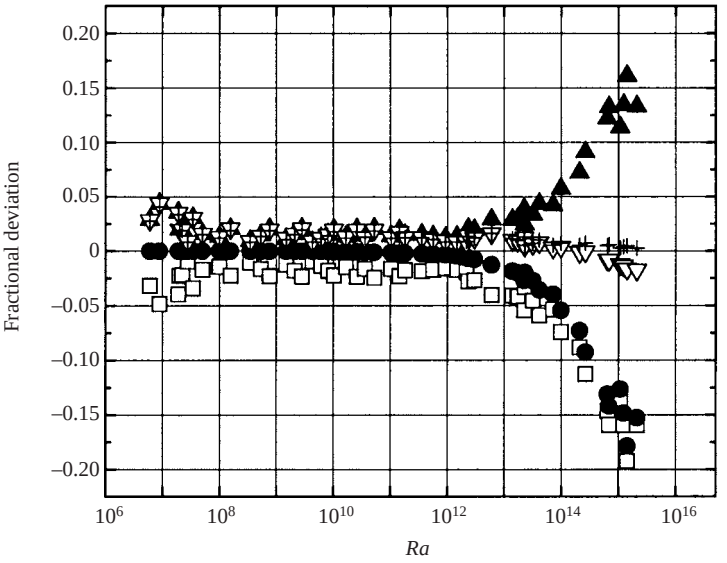

FIGURE 6. The fractional deviation about the mean of various fluid properties for the present data: ●, specific heat, C_P; +, kinematic viscosity, ν; □, thermal expansion coefficient, α; ▲, thermal diffusivity, κ; ▽, thermal conductivity, k_F. These quantities vary by less than 5% for Ra up to 10^{14}, but some of them vary by as much as 20% by $Ra = 10^{15}$.

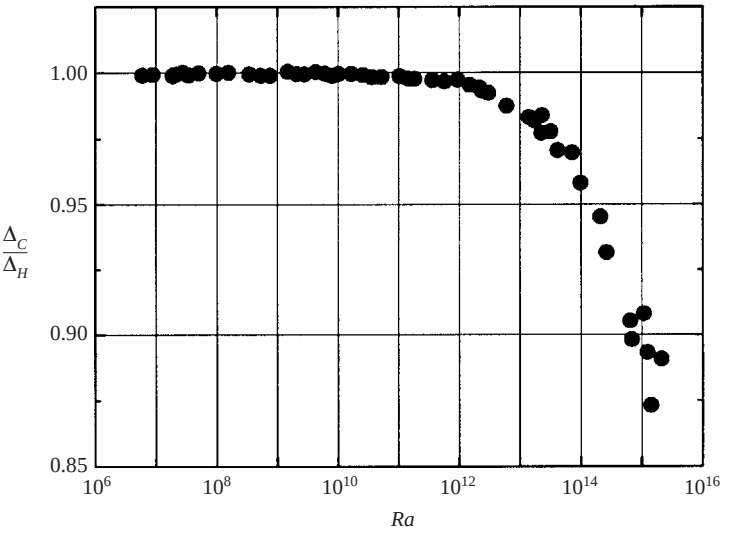

FIGURE 7. The ratio of estimated temperature drops across the top (Δ_C) and bottom (Δ_H) thermal boundary layers defined, from Wu & Libchaber (1991), as $\Delta_C/\Delta_H = [(\alpha_H \nu_C \kappa_C)/(\alpha_C \nu_H \kappa_H)]^{1/3}(k_H/k_C)$. The ratio is a direct measure of the vertical asymmetry and is a measure therefore of non-Boussinesq conditions (see Appendix C for its relation to other measures). In conformity with figure 6, the measure also implies a deviation from Boussinesq conditions of magnitude less than 5% for $Ra < 10^{14}$.

Ra attained with theories of Boussinesq convection. We note that in I, II and the present data the deviation from unity of the non-Boussinesq parameter Δ_C/Δ_H does not occur independently of the average increase in Pr – both effects principally occur

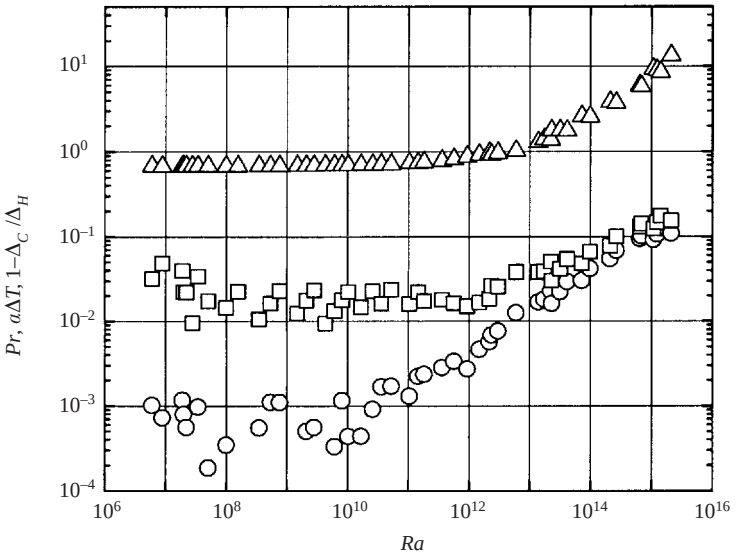

FIGURE 8. The Prandtl number (△) and the parameters $\alpha\Delta T$ (□) and $1-\Delta_C/\Delta_H$ (○), as functions of Ra in the present measurements.

for the same reason in helium experiments, namely a closer approach to the critical point. (There is, of course, no general relationship between Prandtl number and non-Boussinesq conditions.) This is illustrated in figure 8, where two Boussinesq criteria are plotted, together with the Prandtl number, as functions of Ra. A cautionary lesson from here is that the trends in the data that one might be tempted to attribute to an increase in Pr could equally well be correlated with the increase in $1-\Delta_C/\Delta_H$, or vice versa.

6.2. *High-Rayleigh-number convection under stricter Boussinesq conditions*

In the light of this discussion, it is interesting to consider the limiting form of the heat transfer when the asymmetry parameter Δ_c/Δ_H deviates from unity by 5% or less ('stricter Boussinesq'). In figure 9, we plot the Nusselt numbers from the present experiments in such a range. Data from I and II are also plotted for the same range of Ra. The data sets are displaced (by prescribed amounts) for clarity of presentation. In the last decade and a half, all three sets of data in figure 9 (beyond the dotted line) are roughly consistent with a scaling exponent of 1/3 (see, also, Goldstein, Chiang & See 1990). The data in this region are precisely repeatable and are further highlighted by figure 10. In fact, this is just the prediction of Grossmann & Lohse (2001) for their region $\mathrm{IV_u}$, within which, as we have seen in figure 2, both data sets lie. However, questions of whether this region pertains to the infinitely extended and perfectly Boussinesq systems cannot be adequately answered from considerations so far.

7. High-Rayleigh-number convection for criteria under which departures from Boussinesq conditions are large

We have pointed out that measurements towards the high end of Ra correspond to increasingly non-Boussinesq conditions in each of the three measurements (I, II and the present). It should therefore not surprise us if a unique Nusselt number does not

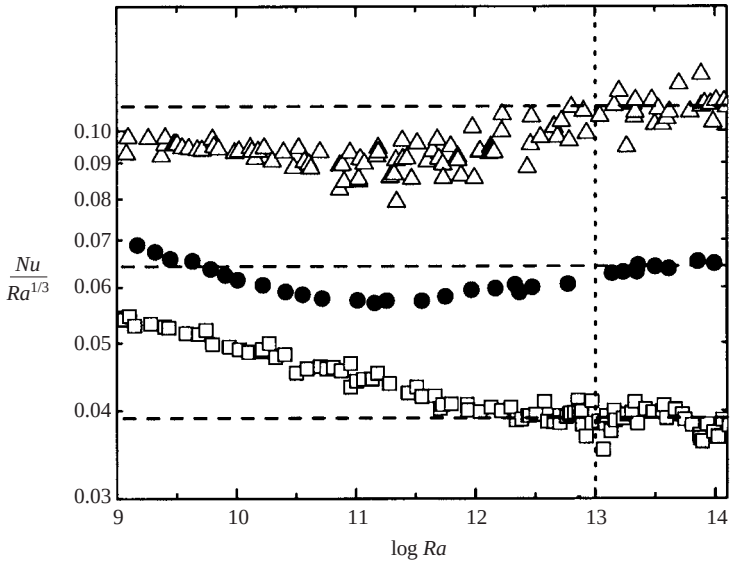

FIGURE 9. Nusselt numbers normalized by $Ra^{1/3}$ for Ra up to 10^{14}. The data sets have been displaced vertically relative to each other for clarity of presentation. □, I (shifted down by 0.02): △, II (shifted up by 0.03); ●, present data (unshifted). All the data are for 'stricter Boussinesq' conditions. For the last decade and a half of Ra (beyond the dotted line), an approximate scaling exponent of 1/3 seems to hold for all three sets of data. This state is attained in different manners in different experiments.

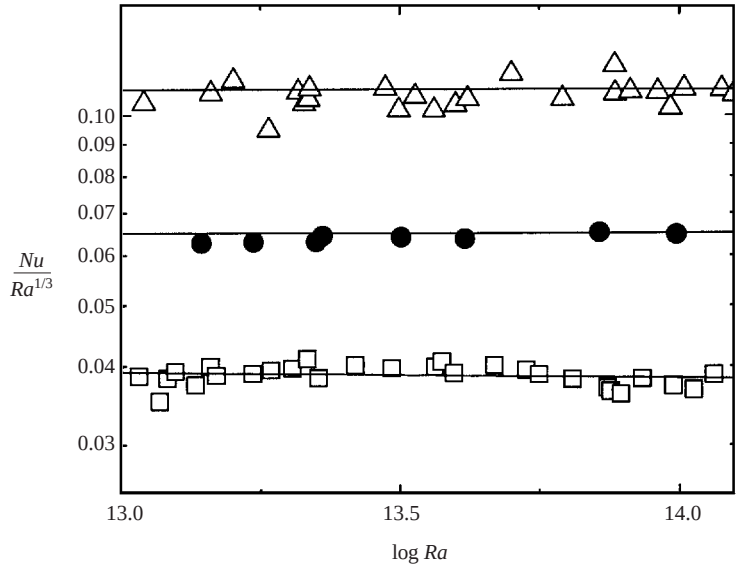

FIGURE 10. Data beyond the dotted line in figure 9 have been expanded here, showing more clearly the 1/3 scaling for the three data sets. As in figure 9, Nusselt numbers are normalized by $Ra^{1/3}$ and displaced vertically by the same amounts as in figure 9. □, I; △, II; ●, the present data.

obtain in this range for a given Ra, Pr and Γ. We can discuss the physics in this high-Ra region only qualitatively.

Let us reconsider the puzzle posed at the beginning of the paper, namely the differences between I and II in the high-Ra range. We expect that no large-scale time-averaged 'modes' of convection are present in this range. This is so because the mean wind, as inferred from measurements, oscillates rapidly – thus averaging over long times to negligible values (Niemela *et al.* 2001*a*; Sreenivasan *et al.* 2002). Yet, the *transient* large-scale motions do set up boundary layers of the type visualized by Kraichnan (1962). The nature of heat transfer must therefore involve changes in the structure of these boundary layers. We consider two limits: one in which the thermal boundary layer is dominated by the shear in the velocity boundary layer, and another in which the former is entirely independent of the latter. The boundary between the two states, however ill-defined in practice, is of some interest for the present discussion.

7.1. *Boundary layer thickness ratios*

The thickness of the thermal boundary layer is given by the well-known formula

$$\lambda/H = 1/(2Nu). \tag{7.1}$$

It is perhaps useful to note that the formula rests on the simplistic assumption that the temperature distribution in the boundary layer can be approximated by a linear distribution with the correct slope at the wall. If we use Howard's (1966) model to write

$$\lambda = H(Ra_c/Ra)^{1/3}, \tag{7.2}$$

where Ra_c is the critical Rayleigh number for the onset of convection, and take Ra_c to be $O(10^3)$, as did Howard, we obtain

$$\lambda/H \approx 10/Ra^{1/3}. \tag{7.3}$$

There is, of course, no serious justification for using Howard's estimates, so we may use, instead of (7.3), equation (7.1) with Nu taken from measurements.

The velocity boundary layer thickness can be defined in at least two ways. One definition is through the mean velocity gradient at the wall, analogous to that of the thermal boundary layer thickness through the wall gradient. Denote this thickness by δ_1. More precisely, δ_1 is the distance from the wall where the two straight lines, one tangent to the velocity profile at the wall, and another tangent to it at the position of maximum velocity, meet. (The position of maximum velocity, to be denoted by δ, defines the boundary layer thickness in the classical sense of Prandtl; we will exploit this feature in Appendix F.) A second definition is through the distance at which the turbulent shear stress in the boundary layer is equal to the viscous stress. Nominally, turbulent fluctuations will not penetrate closer to the wall than this thickness, denoted here by δ_2. In Appendix F, it is shown that

$$\delta_1/\lambda = 634\Gamma^{0.137}NuPr^{0.603}/Ra^{0.423}, \tag{7.4}$$

and

$$\delta_2/\lambda = 648\Gamma^{0.091}NuPr^{0.636}/Ra^{0.445}. \tag{7.5}$$

Both equations have a similar structure, which is reassuring. If we use the empirical fit obtained in I for Nu, we obtain, for instance,

$$\delta_2/\lambda = 76Pr^{0.636}/Ra^{0.136}. \tag{7.6}$$

The condition corresponding to the unity value for δ_2/λ in the (Pr, Ra)-plane is given by

$$Pr = Ra^{0.214}/905, \tag{7.7}$$

which is very similar to that of Malkus (2001), namely

$$Pr = Ra^{0.167}/140, \tag{7.8}$$

obtained from different considerations. The two numerical values (7.7) and (7.8) are quite close for a range of Rayleigh numbers, and to the boundary for the crossing of the viscous and thermal boundary layers deduced by Shraiman & Siggia (1990). The latter is given approximately by

$$Pr = (Ra/10^{13})^{1/4} \tag{7.9}$$

where the normalizing Ra of 10^{13} is taken roughly halfway within the range given by those authors ($3 \times 10^{12} - 2 \times 10^{14}$).

The unity value of δ_1/λ or δ_2/λ can be thought to distinguish the shear-dominated conditions near the wall from those dominated by thermal plumes. Thus, when both Ra and Pr vary in an experiment, whether or not one attains the shear-dominated regime depends roughly on the relative rates of variations of Ra and Pr – according to $Pr/Ra^{0.214}$, say, taking the estimate of (7.7) as the example. The ratio δ_2/λ attains unity value in I roughly for $Ra \sim 10^{14}$ – the values of this ratio for II and the present data are approximately 4 and 2.5, respectively. Thus, the boundary layer in I is close to being shear-dominated whereas that in II is more responsive to plumes and thermals. (The present case lies in between.) For the plume-dominated case, we remark incidentally that Howard's (1966) estimate of an upper bound for the heat transport, given by

$$Nu = 0.126R^{3/8}. \tag{7.10}$$

comfortably bounds the data.

We have plotted in figure 11 the three data sets in the (Pr, Ra)-plane together with equations (7.7)–(7.9). This comparison supports the conclusion that I is more likely to be shear-driven and II thermally driven, and suggests that Kraichnan's theory might be more appropriate to I than to II. Interestingly, this is not contradicted by the data of I: even though they yield a constant slope close to 0.31, they are consistent with Kraichnan's formula ($Nu \propto Pr^{-1/4}Ra^{1/2}/[(\log Ra)^{3/2}]$), because the Pr and $\log Ra$ terms together yield an effective asymptotic slope of 0.315 over the ranges of Ra and Pr covered in I.

7.2. *Comments on heat transport in very high-Ra experiments*

Since the conditions corresponding to Kraichnan's 'ultimate state' appear, from these considerations, to be more applicable to I than to II, we are now left to explain why II measures a larger heat transport for $Ra \gtrsim 10^{12}$ than either I or the present experiments. This paradox can be understood from a further consideration of the relative thicknesses of the velocity and thermal boundary layers.

The velocity boundary layer has a certain fraction of its thickness near the wall within which the transport occurs principally by viscous action. If the thermal boundary layer is entirely embedded in this part of the velocity boundary layer, it is natural to think that the turbulence in the boundary layer would have little impact on heat transport. On the other hand, if the two thicknesses are comparable, or if the turbulent velocity boundary layer is embedded in the thermal layer, the

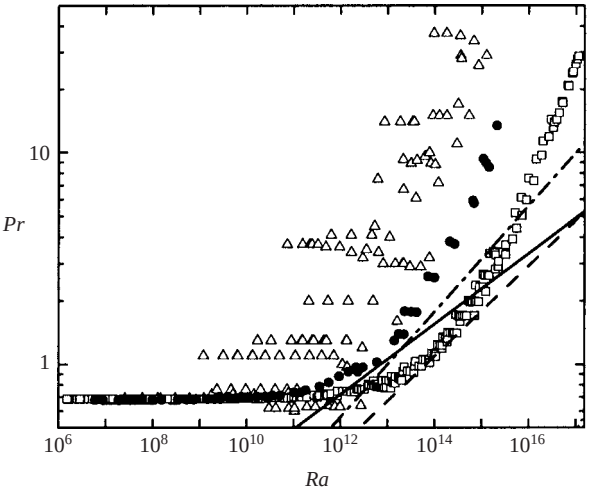

FIGURE 11. The variation of *Pr* with *Ra* for the three experiments shown in figures 3 and 4. □, I; △, II; ●, the present data. For $Ra > 10^{10}$, all three sets of data lie essentially in the same sub-region IV_u of Grossmann & Lohse (2001) (see figure 2). The solid line is Malkus's expression (7.8) for unity value for the ratio of the velocity boundary layer to the thermal boundary layer. The dashed line marks the same condition for the ratio δ_2/λ (see (7.7)). The two lines are quite similar, especially if we allow for the uncertainty in these estimates. Also shown is the boundary (7.9) according to Shraiman & Siggia (dot-dashed line). The various lines suggest that I may be closer to forced convection and II may correspond more closely to free convection. The present data lie in between.

transport may be expected to be influenced strongly by boundary layer turbulence. The ratio of the thicknesses of the two boundary layers depends on *Pr*.

In the intermediate-Rayleigh-number range, as well as that portion of the higher-*Ra* region where stricter Boussinesq conditions prevail, the available evidence indicates that the *Pr*-dependence is negligible (see § 5). But, for very high *Ra*, the state of the boundary layers in I, II, as well as present experiments is continually changing because both *Ra* and *Pr* change simultaneously. It is therefore not obvious that the *Pr*-dependence would be negligible. Kraichnan (1962) built these effects into his results, but emphasized that the estimates were uncertain. His main qualitative message, however, is that the heat transport is promoted if the Prandtl number is low.

Kraichnan's work considers the case when boundary layer fluctuations reach all the way into the thermal boundary layer so that all parts of it are influenced by turbulent fluctuations. However, it is unclear *a priori* if this enhances or inhibits heat transport. While the generation of small scales in the boundary layer would enhance heat transport (as Kraichnan assumed), the nearness to the boundary will also restrict the vertical scale of convective movements and thus inhibits heat transport (Townsend 1959). It is thus possible that the largest amount of heat transport in these experiments may not be associated with boundary layer fluctuations expected for lower Prandtl number (as visualized by Kraichnan), but rather by the converse: for large *Pr*, the thermal boundary layer does not feel the effects of small-scale fluctuations, and would behave essentially as that on a flat plate with no mean flow at its exterior. This is akin to the case of pure free convection, for which plumes are the most favoured form of heat transport (see, for example, Sparrow, Husar & Goldstein 1970). Visual observations of thermal convection suggest that plumes not only transport heat effectively, but also produce large-scale velocity fluctuations. It is plausible then that

the heat transport generated in this way is stronger than the enhancement due to fluctuations in boundary layer turbulence.

8. Conclusions

Numerous discussions among experimental groups have moved the focus away from differences between experimental apparatus or procedure as the sources of primary differences among the few high-Ra data. The new data support this conclusion and redirect attention to flow physics. In this context, it appears to us that the confinement of convection plays a significant role in determining the state of the flow at moderately high Ra, and theories of infinitely extended convection may not apply in precise detail to the high-Rayleigh-number experiments of recent origin.

This paper has several thrusts. First, we have highlighted in the intermediate-Ra range the large differences among different experiments (exceeding experimental uncertainties) and noted that the Nu data lie mainly in two bands as Ra varies. The two bands are not correlated individually with either the Prandtl number or the aspect ratio. That two experiments in the same apparatus and at nearly constant Pr yield measurably different results at comparable Ra appears to rule out errors of procedure; that the aspect ratio in itself is not the primary factor is supported by the fact that the trend with aspect ratio could be different in different experiments (contrast Wu's data for $\Gamma = 1$ and $1/2$ with I and the present data). This supports the conclusion of Roche *et al.* (2002) that different large-scale (time-averaged) modes of convection may be responsible for the two rough groupings of the Nu data. The large-scale motion might itself be related in detail to the Prandtl number, the construction of the apparatus, the aspect ratio and so forth, but these details themselves do not matter directly.

We have examined the criteria for Boussinesq conditions and noted that little is known about the consequences of strong non-Boussinesq conditions far from equilibrium. Further, we have shown that the large and systematic departures at high Ra and the sharp increases in Pr are not independent of each another in existing high-Ra data, because they are both the result of approaching the thermodynamic critical point of the working fluid. It is thus difficult to correlate changes in Nu with a simple combination of Ra and Pr, or Ra and a non-Boussinesq parameter such as Δ_C/Δ_H.

Since there is the likelihood that non-Boussinesq effects could affect heat transport in unknown ways, we asked two questions: (*a*) What is the nature of the heat transport at the highest Rayleigh numbers measured and for which stricter Boussinesq conditions hold? (*b*) For conditions under which non-Boussinesq effects may not be negligible, what qualitative remarks can be made concerning heat transport? Our considered response to (*a*) is that all the data seem to be approximately consistent with the classical power-law exponent of $1/3$ (though we do not rule out slow variations around this value) and with the prediction of Grossmann & Lohse (2001) for region $\mathrm{IV_u}$ of their phase plane. The possible correspondence with the classical theory does not surprise us because the mean wind has become less effective in this range (thus possibly removing the height of the apparatus as a parameter in the problem), but we are aware that this conclusion needs to be set on a firmer foundation by new measurements. With respect to (*b*), which includes the puzzle concerning the differences at very high Ra between I and II, it is clear that an additional consideration is needed. We have argued qualitatively that the main difference is that I is closer to being shear-driven, while II may be closer to being thermally driven. We have further

argued that the shear-dominated case does not necessarily lead to the largest heat transfer. This conclusion is based on relative thicknesses of the velocity and thermal boundary layers.

The overwhelming lesson to be drawn from the work is that the experiments in containers of small aspect ratio cannot be compared, without quantitatively understanding the myriad details associated with finite size effects, to theories that presume infinite lateral extent. No high-Ra experiment to-date has been made at constant Pr and under stricter Boussinesq conditions so they can be compared to theories that assume perfect vertical symmetry. On the other hand, we have learnt a great deal from low-aspect-ratio measurements. For example, the Nusselt number at a fixed Ra may depend measurably on the strength and steadiness of the mean wind – but not on every detail such as the aspect ratio, geometry of the apparatus and the Prandtl number. The complexity is that we do not yet understand the precise way in which these and other details determine the mean wind. A beginning has been made in Sreenivasan *et al.* (2002).

An obvious corollary is that the next generation of heat transport measurements are best made in apparatus of large aspect ratio.

We thank L. Skrbek and R. J. Donnelly for continued collaborative work. We have benefitted from numerous discussions with many colleagues, of whom we mention a few: G. Ahlers, A. Bershadskii, B. Castaing, X. Chavanne, S. Grossmann (especially), R. M. Kerr, D. Lohse, H. Meyer, P. Roche, P. Tong and R. Verzicco. The research was supported by NSF grant DMR-95-29609.

Appendix A. The transition Rayleigh number

The Rayleigh number marking the transition of the boundary layer to the turbulent state can be estimated as follows. This is of some interest because the nature of the boundary layer is an important ingredient of the understanding of the flow; see, for example, Shraiman & Siggia (1994) and Grossmann & Lohse (2000). The most appropriate parameter characterizing the state of a boundary layer is its momentum-thickness Reynolds number, $R_\theta = V_M\theta/\nu$, where V_M is the mean wind speed and θ is the thickness measuring the momentum loss due to the velocity deficit in the boundary layer. Although the boundary layers on the top and bottom walls are not as clean as those studied on flat plates in the fluid dynamics literature, one can obtain some estimates by invoking this idealization. The boundary layer will be considered here to have started at a corner, from where it is assumed to develop on the top (or bottom) wall. This picture is not too unrealistic, because the ratio of the diameter of the apparatus to the boundary layer thickness is relatively large: at $Ra = 10^{12}$, this ratio is of the order 100. We are interested in the state of the boundary layer nominally at the mid-point of the bottom and top plates. Thus, the streamwise development length x is taken to be $D/2$, where D is the diameter of the apparatus. This picture ignores a number of details, but is nevertheless helpful for making plausible estimates. A simple fit to the flat-plate boundary layer data (e.g. Wieghardt & Tillmann 1951) shows that the momentum-thickness Reynolds number of the boundary layer is related to the Reynolds number based on the streamwise distance x by

$$R_\theta \approx 0.019 R_x^{0.864}. \tag{A 1}$$

More sophisticated fits have been used in the literature, but this simple fit will suffice here. Noting that the Reynolds number $R_x = R_{D/2} = \frac{1}{2}R_D = \frac{1}{2}\Gamma R_H$, where, following

convention, the bulk Reynolds number R_H is based on the height H of the apparatus, we can relate R_θ to R_H. Using the empirical result, whose basis will be described in Appendix D, that $R_H \approx 0.2Pr^{-0.7}Ra^{0.49}$, we may rewrite the above equation as

$$R_\theta \approx 2.64 \times 10^{-3} \Gamma^{0.864} Ra^{0.423} Pr^{-0.605}. \tag{A 2}$$

Needless to say, the applicability of (A 2) is limited to the range for which the formula for R_H is valid. It is well-known in the turbulence literature (e.g. Preston 1958; Narasimha & Sreenivasan 1979) that a boundary layer cannot be maintained turbulent for R_θ below about 320 because the production of turbulent energy would then fall below the rate of its dissipation. By using this value of R_θ in (A 2), we determine that

$$Ra^* \approx 5.66 \times 10^{11} Pr^{1.4}/\Gamma^2 \tag{A 3}$$

marks the minimum Ra for the boundary layer to be turbulent. There are issues concerning the aspect ratio that are not taken into account fully in this discussion, so (A 3) is to be regarded only as a rough guide for distinguishing the turbulent state of the boundary layer from the non-turbulent state. Equation (A 3) is drawn in figure 2 as the long-dashed line. Other estimates using different criteria have been made by Grossmann & Lohse (2000, 2001, 2002), and are also plotted in figure 2.

Appendix B. Effects of sidewall conduction

Some fraction of heat is always conducted from the bottom plate to the sidewall. A proper evaluation of the Nusselt number requires that the effect of this 'heat leak' be understood correctly. Naively, one may subtract the amount of heat transmitted through the sidewall by assuming a linear temperature gradient from top to bottom and calculating the empty-cell conduction. This commonly used procedure is inadequate in principle because the temperature distribution along the height of the sidewall is not linear when the flow is turbulent but is sharp near the top and bottom walls. Thus, the heat lost from the bottom plate to the sidewall in the vicinity of their contact can be expected to be significantly larger. However, this heat cannot be conducted directly through the sidewall all the way to the top plate, because the temperature gradient becoms negligible in the middle. Most of the heat must thus flow back laterally into the fluid very near the horizontal boundary within a distance that probably scales with the boundary layer thickness (see Roche *et al.* 2001), and flow yet again into the sidewall near the top plate. Thus, nearly all the heat injected into the bottom plate takes part in the convection process, and very little of it goes straight through the sidewall. One may thus imagine that the effect of sidewall conduction is not major. If so, the heat that is directly transported through the sidewall may well not be much different from that given by the empty-cell approximation. This seems to be borne out by comparisons of the Nusselt numbers measured in the empty-cell approximation with those calculated by integrating the turbulent heat transport across the apparatus (Verzicco 2002).

These two answers, even if they agree with each other, must do so for the wrong reasons if our interest is in the problem of 'ideal' convection for perfectly insulated walls. The quest then is to determine the effects of the complicated heat path on the physics of turbulent thermal convection.

These problems have received attention by Ahlers (2001) and Roche *et al.* (2001), who have devised approximate schemes to account for the sidewall conduction effects.

In an unpublished note stimulated by Ahlers' work, Sreenivasan (2000) simulated aspects of the problem using a simplified flow model. Verzicco (2002) has done a more complete analysis for aspect ratio 1/2 and $Pr = 0.7$. Considering the lower portion of the cell, Verzicco indeed observed that some fraction of the heat is conducted into the sidewall from the bottom boundary and then conducted back into the fluid a short distance above. As already mentioned, the Nusselt numbers obtained by integrating the turbulent stresses over the entire volume of the fluid are close to those measured for comparable conditions using the empty-cell approximation.

However, this is not the entire answer because the Nusselt numbers obtained in this way are substantially larger than those for perfectly non-conducting walls, i.e. when both inner and outer surfaces of the sidewall are non-conducting. This enhancement is attributed to the forcing of the large-scale wind when heat is transported into the fluid (near the bottom plate) and out of it (near the top plate). For Rayleigh numbers where the enhancement is largest, it has been demonstrated (Verzicco & Camussi 2003) that the mean flow consists of strong toroidal roll structures near the top and bottom plates and a weaker overall circulation spanning the cell. At higher *Ra*, the toroidal structure loses dominance to the full-scale mean wind. Furthermore, the toroidal rolls have only upflow at the bottom heated surface and only downflow at the top cooled surface, so that the effect of lateral heat currents near the boundaries can be seen to greatly enhance the buoyancy of such flows.

For aspect-ratio-unity cells, the same simulations (Verzicco & Camussi 1999) show that only the large-scale circulation around the cell circumference is dominant and therefore the above arguments do not necessarily apply, that is the mean wind would be subject to both enhanced and depleted buoyancy from sidewall currents. This was proposed as an explanation for the occasional reversals of the mean flow direction by Sreenivasan *et al.* (2001). In fact, it was shown there that a quantitative agreement existed between the temperature equilibration time for the corner region of the flow, defined in terms of the exponential thermal length scale of Roche *et al.* (2001) on the one hand, and the upper cutoff scale for the probability density function of direction-switching intervals for the mean flow on the other. We further point out that when a mylar sheet was glued to the fluid–wall interface, the threshold for mean wind reversals was shifted substantially upward in *Ra*, indicating that the strength of lateral heating – which can upset the delicate balance between enhanced and depleted buoyancy – was reduced.

Although much is understood about the effect of sidewall conduction, it is useful to summarize, for three reasons, the results of the numerical solution of the idealized problem studied by Sreenivasan (2000). First, the solution considered the heat transfer problem for the combination of the fluid and the container as it corresponded to our particular experiment; second, it introduced the mean wind, whose importance we have already considered, as an explicit part of the problem. Third, the model allowed some estimates to be made even at the highest Rayleigh numbers measured.

A schematic of the idealized flow is shown in figure 12, where it is assumed that the flow is two-dimensional. The flow recirculates through the annular region continually, resembling the mean wind which is prescribed from measurement. The mean flow is allowed to vary according to measurement but its form does not change with *Ra*. The boundary layers are assumed to be laminar. This idealization was motivated by the fact that the corrections are negligible for Rayleigh numbers exceeding 10^{11}, below which the Reynolds number of the mean wind is small enough for the boundary layers to be non-turbulent (see Appendices A and D). However, the heat transport

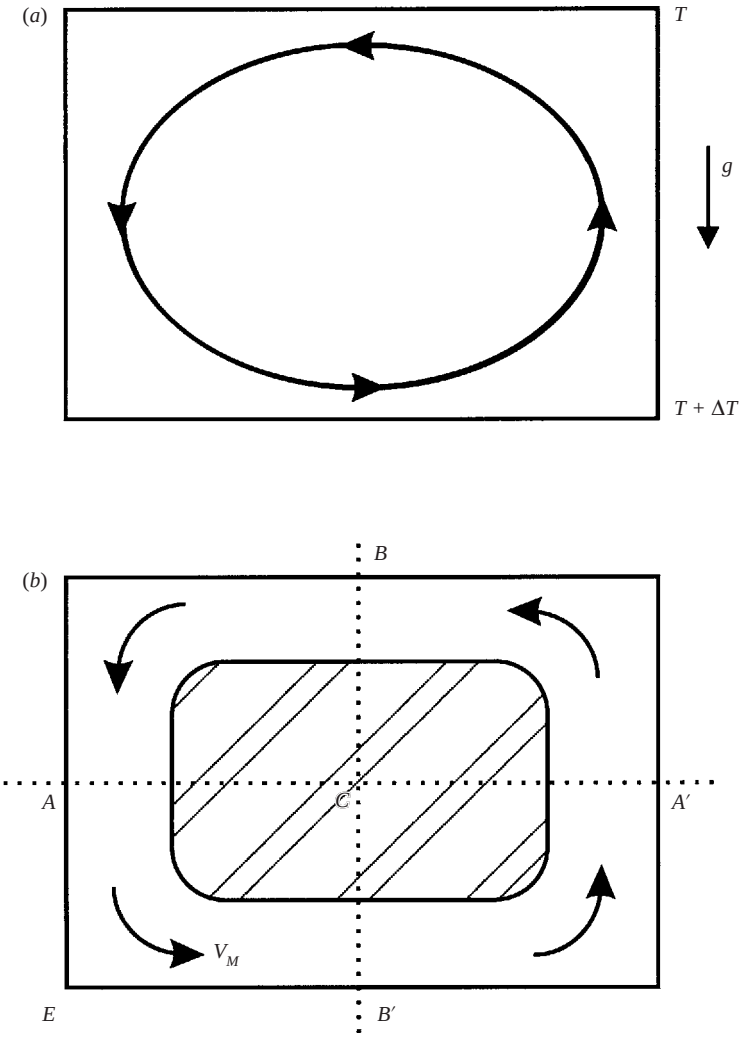

FIGURE 12. Schematic of (*a*) the mean wind at high Rayleigh numbers and (*b*) the idealized problem solved by numerical simulations. The hatched region is assumed not to participate in the flow. The rounding of the corners has been varied by a factor of two with no perceptible changes in the heat transport results.

characteristics of the laminar boundary layer, including that in the corner regions, are part of the solution. The central core is disregarded on the premise that, when the recirculating motion is strong, it may be enough to simulate the flow fairly close to the walls (though, on the scale of the boundary layer, it would exceed many times its extent), without concerning ourselves with details in the core. As remarked already, the problem was solved in conjunction with the actual dimensions and properties of the top and bottom plates, the sidewall material properties (including flanges) and the properties of the helium gas. Numerical simulations were performed using commercial FLUENT code 5.0.2. For reasons of symmetry about the axes AA' and BB' (see figure 12), calculations were made for only one quarter of the cell $ACB'E$ (aspect ratio unity). Between 100×10^3 and 400×10^3 numerical grid points were used to solve both the boundary layer and the associated heat transfer. The results show that the

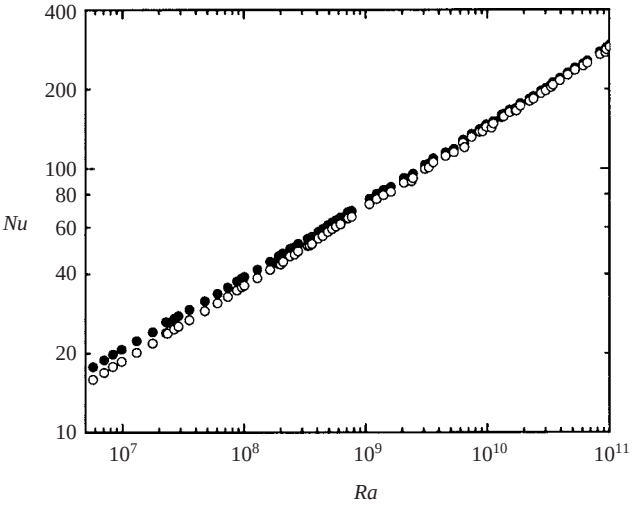

FIGURE 13. The Nusselt number data, obtained for the case of bare stainless steel walls bounding the fluid, corrected according to the results of numerical simulations. ●, Uncorrected *Nu*; ○, corrected *Nu*. The correction is negligible beyond *Ra* of about 10^9. The correction schemes devised by Ahlers (2000) are similar though the magnitudes are somewhat larger.

velocity gradients are largest near the corner. While the precise details are influenced by details of geometry, one feature that stands out in the flow is the formation of strong corner eddies in the flow.

Figure 13 shows the Nusselt numbers obtained for the case of bare stainless steel walls bounding the fluid modified according to this correction scheme. This correction suggests that the various published Nusselt numbers at low *Ra* are overestimated. The result is a slightly larger effective local slope in the power law than is estimated from the raw data. Even though the present simulations attempt to replicate the properties of the entire system, and the boundary layers are explicitly obtained as part of the solution, the various approximations in the model imply that the corrections cannot be precise. All that one can say is that the correction shifts a range of *Nu* downward by a few percent and that this shift diminishes as the Rayleigh numbers increases. It is notable that the thickness of the sidewall is unimportant in the simulations, i.e. the existence of flanges adjacent to the fluid layer has no measurable effect on the amount of correction suggested.

Details of the flow are quite complex, and the corner flow makes the situation even more so. We surmise that the stagnant fluid within the corner eddy will continually be heated from the bottom wall until it takes off as a large plume and disposes off the excess heat partly into the bulk of the fluid and partly back into the sidewall. The fraction of heat that these corner eddies transmit to the sidewall, in relation to the amount that they discharge into the bulk of the fluid, depends on the ratio of the thermal conductivity of the sidewall to that of the fluid. In general, the size of the corner eddies does not scale simply with Reynolds number (and thus with *Ra*), so the relative effect depends on *Ra* and the detailed geometry. The criterion for negligible sidewall conduction seems to be that the sidewall conductivity should be small compared to the molecular conductivity of the fluid. For convection studies in helium, the thermal conductivity of the gas is typically of the order of 10^{-2} W m^{-1} K^{-1}. The conductivity of the sidewalls should be smaller still. No high-*Ra* helium gas

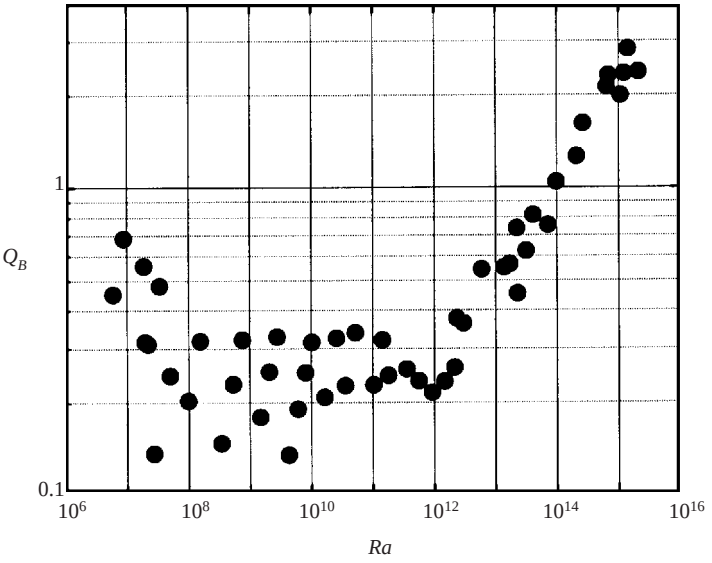

FIGURE 14. The Boussinesq parameter Q_B, as defined in the text, for the present data as a function of Ra.

experiment to-date satisfies this stringent requirement. Typically, the stainless steel sidewalls used in these experiments have a conductivity of the order of 0.25 W m^{-1} K^{-1}, this being about an order of magnitude larger than that of the gas. As the Rayleigh number increases, of course, the constraint becomes less stringent because the molecular transport of the fluid is augmented strongly by the turbulent transport.

Appendix C. Further details on non-Boussinesq effects

Busse (1967) has constructed a weighted measure $Q_B = \sum c_i \Psi_i$ to reflect the degree of compliance of the Boussinesq approximation, where Ψ_i represents the fractional deviations of fluid properties and the coefficients c_i depend on the Prandtl number. It is not clear whether this measure applies to high-Rayleigh-number convection, but it may still be useful as a qualitative indicator. We expect Q_B to be of order unity or less for the Boussinesq approximation to hold. Figure 14 shows that this condition holds up to Ra of order 10^{14}, consistent with the statements on other Boussinesq measures in § 6.

Most experiments on convection have not considered the non-Boussinesq effects in detail. A rule of thumb used in I and II (with some restrictive justification) is that the Boussinesq approximation holds whenever $\alpha\Delta T < 0.2$. It is helpful to relate the criterion based on $\alpha\Delta T$ to those based on Q_B and Δ_C/Δ_H, since fluid properties are not always available in the published literature for computing either of these more complex parameters. We therefore plot $\alpha\Delta T$ against Q_B in figure 15 and against Δ_C/Δ_H in figure 16. Not unexpectedly, all the data for $Ra \lesssim 10^{14}$ lie near the origin in both figures, and the data in the increasingly non-Boussinesq region lie very nearly on the following straight lines:

$$Q_B \approx 0.062(\alpha\Delta T), \quad \Delta_C/\Delta_H \approx 1.25(\alpha\Delta T). \tag{C 1}$$

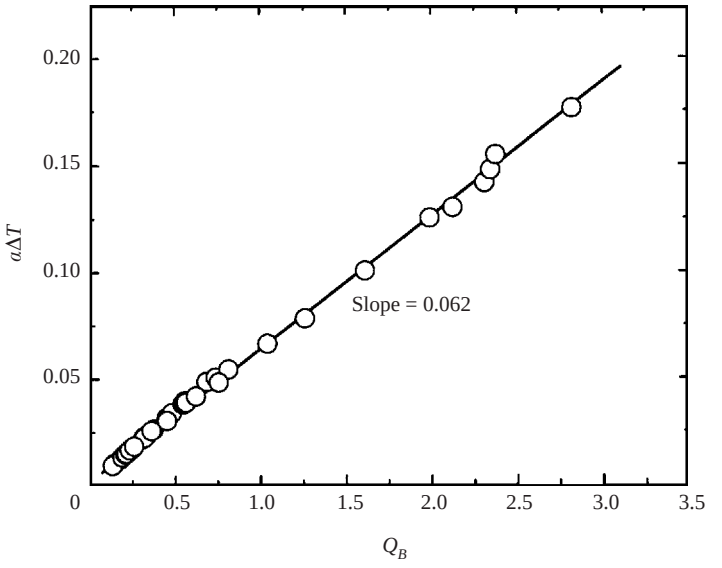

FIGURE 15. $\alpha\Delta T$ as a function of the Boussinesq parameter Q_B defined by Busse (1967) for the present data. A linear relation holds with slope 0.062.

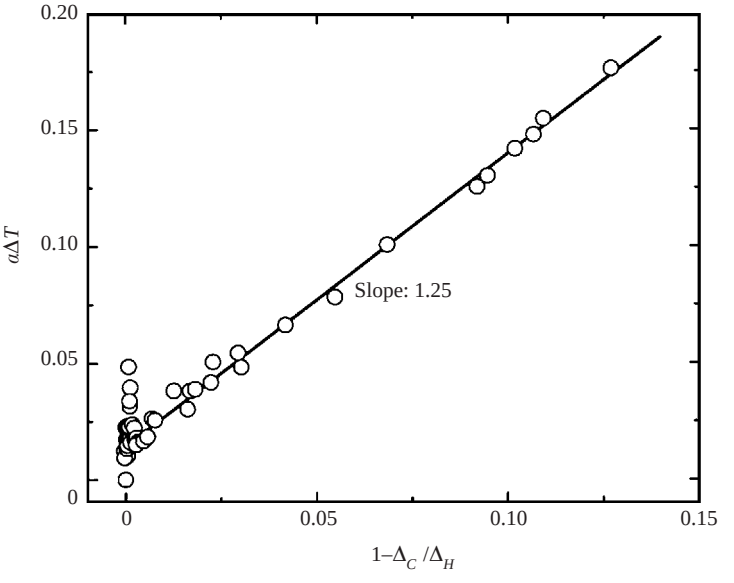

FIGURE 16. $\alpha\Delta T$ as a function of $1 - \Delta_C/\Delta_H$ for the present data. A linear relation holds with slope 1.25.

It is reassuring that simple relations exist between $\alpha\Delta T$ on the one hand and the more complex quantities Q_B and Δ_C/Δ_H on the other. This suggests that, in principle, one can use $\alpha\Delta T$ instead of the other two, both of which require more detailed knowledge of flow parameters. It is, of course, possible that these empirical relations are not universally valid for all experiments, but we expect the general features to carry over.

Appendix D. The mean wind

In convection studies with relatively large aspect ratio, Krishnamurti & Howard (1981) observed a component of motion spanning the entire transverse dimension of the apparatus, bridging all the large-scale convection cells present in it. For aspect ratios of order unity, the mean wind is correlated over the entire apparatus (e.g. Sano, Wu & Libchaber 1989; Castaing *et al.* 1989; Cioni, Ciliberto & Sommeria 1996; Takeshita *et al.* 1996; Xin, Xia & Tong 1996; Niemela *et al.* 2000*a*; I; II; Sreenivasan *et al.* 2002). It is this mean wind that permits well-formed velocity and thermal boundary layers to occur on the walls of the container. The wind changes direction relatively abruptly at high Rayleigh numbers (e.g. Niemela *et al.* 2001*a*; Sreenivasan *et al.* 2002), but the essential element is that it is sustained in one direction or another for long periods of time to enable a Reynolds number $R_H = V_M H/\nu$, where V_M is the velocity of the mean wind, to be defined and boundary layers to be formed on the walls of the container. From our measurements we find the Ra dependence (we will consider the addition of Pr below) to be

$$R_H \propto Ra^{0.47}. \tag{D 1}$$

The exponent can be somewhat smaller or larger in various other experiments, but this difference may be due to differences in the measurement techniques employed.

The dependence of Re on Pr has not yet been appreciated fully. To see this dependence, we consider the experiments of different authors at different Prandtl numbers. Takeshita *et al.* (1996) and Cioni *et al.* (1997) measured the Reynolds number in the convection of mercury ($Pr = 0.025$). Similarly, Castaing *et al.* (1989), and I and II measured the Reynolds number for helium gas; although Pr in their measurements increased towards the high-Rayleigh-number end, say for $Ra > 10^{12}$, we shall consider here their data for lower Ra for which $Pr = 0.7$. Sano *et al.* (1989) and Xin *et al.* (1996) used water with $Pr = O(5)$. Finally, Ashkenazi & Steinberg (1999) used SF_6 with varying Pr up to about 190. If we select representative data from each experiment and plot the measured Reynolds number against Pr at a fixed Ra of 10^{10}, we obtain figure 17. It is clear that a power-law with an exponent of -0.7 is plausible. Considering the extrapolations involved, we cannot be certain that the magnitude of the true power-law exponent, if one exists, is not a close rational number such as $2/3$ or $3/4$. That the dependence is non-trivial is all that can be said with confidence. This is particularly so because the aspect ratio among the experiments varies between $1/2$ and 1. That effect is not easy to assess.

Taking figure 17 into account, a reasonable fit to the Reynolds number data for the experiments considered here is

$$R_H = f(\Gamma) Pr^{-0.7} Ra^{0.49}, \tag{D 2}$$

where the factor $f(\Gamma)$ allows for the dependence on the aspect ratio. The many prevailing uncertainties in available measurements prevent us from determining its magnitude accurately, but it is about 0.2 for aspect ratios of order unity.

Appendix E. Correlation with energy dissipation

To the lowest order we can correlate the various data sets with the energy dissipation in the convection apparatus. We can write down a simplified relation for the dimensionless dissipation as

$$(Nu - 1) Ra/Pr^2 \propto Re^m, \tag{E 1}$$

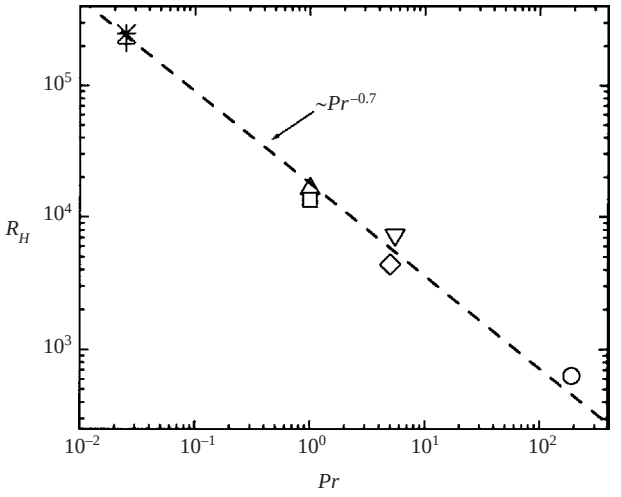

FIGURE 17. The variation of the bulk Reynolds number R_H, for Ra held fixed at 10^{10}, versus Pr from various sources of data: □, I; △, II; ○, Ashzenazi & Steinberg 1999, extrapolated; ▽, Xin *et al.* 1996; ◇, Sano *et al.* 1989; +, Cioni *et al.* (1997), extrapolated; ∗, Takeshita *et al.* (1996), extrapolated. The line marks $R_H \approx 1.8 \times 10^4 Pr^{-0.7}$.

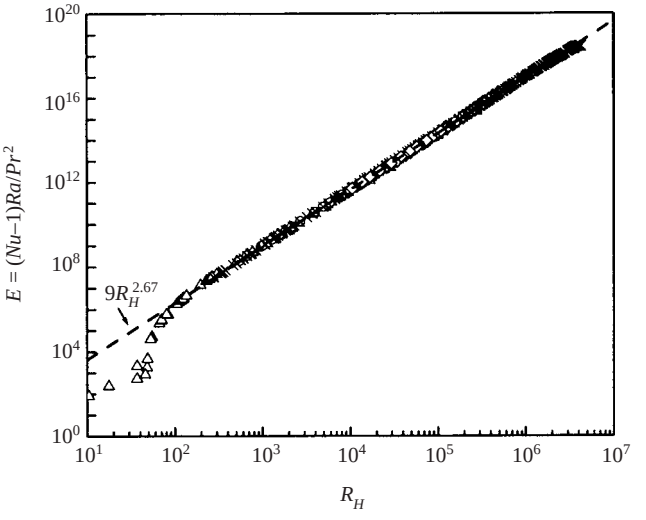

FIGURE 18. The dimensionless dissipation $(Nu - 1)Ra/Pr^2$ as a function of $R_H = 0.2Ra^{0.49}Pr^{-0.7}$. The average dissipation is given to good approximation by the line $9R_H^{2.67}$ over a large range of values. △, II; ○, present data; ×, I; ⋆, $Pr = 0.7$, Roche (2001); ▽, $Pr = 1.5$, Roche (2001); ◇, $Pr = 1.1$, Roche (2001).

where $m = 3$ for turbulent dissipation and 5/2 for the laminar. Grossmann & Lohse represent the general form for the dissipation as a linear combination of terms involving the exponents 3 and 5/2. In figure 18 we plot $(Nu - 1)Ra/Pr^2$ versus the Reynolds number associated with the mean flow given by (D 2) for a number of recent high-Ra experiments in helium gas. Taking a common prefactor of 0.2 in (D2)

for all data sets, we may write

$$NuRa/Pr^2 \approx CRe^{2.67}. \tag{E 2}$$

Excellent collapse of all experimental data is found for over 4 decades of Reynolds number (corresponding to about 8 decades of Ra). The proportionality constant in (E 2) is about 9. Similar to our earlier discussion of Nu, (E 2) with $C = 9$ seems, then, a reasonable characterization for the dimensionless dissipation to the highest Ra for which stricter Boussinesq conditions hold. Since the scaling of the dissipation is related to that of Nu, this may be regarded as giving the lowest-order approximation of Nusselt number that ignores the various details affecting Nu in the low- and intermediate-Ra regimes. Interestingly, the data of Creveling *et al.* (1975) obtained in an analogous experiment involving convection in a heated circular loop follow the same form in the turbulent regime and agree well quantitatively with this result. Though one should not trust all the detailed implications of this observation, we believe the result may be usefully, though cautiously, extrapolated.

Appendix F. Further details on boundary layer development

Some of the critical relations needed to obtain (7.4) and (7.5) are noted here. From the definition of δ_1, it is easy to show that

$$\delta_1/\delta = 2/(c_f R_\delta), \tag{F 1}$$

where c_f is the skin friction coefficient ($\equiv \tau/\rho V_M^2$, with τ and ρ the shear stress at the wall and the fluid density, respectively) and $R_\delta = V_M\delta/\nu$, δ being the conventional definition of the boundary layer thickness used in aerodynamics, namely the distance from the wall where the velocity reaches some prescribed fraction such as 99% of the maximum velocity, V_M. Writing

$$\delta_1/H = (\delta_1/\delta)(\delta/H), \tag{F 2}$$

and using (F 1) and the standard boundary layer correlations for the second ratio on the right-hand side, one may obtain the ratio δ_1/H. This required correlation can be obtained, for example, from the analysis of the boundary layer data of Wieghardt & Tillmann (1951) at high Reynolds numbers. From this analysis we have

$$c_f R_\delta \approx 0.0169 R_\delta^{0.84}, \quad R_\delta \approx R_x^{0.854}/7, \tag{F 3}$$

where x is the distance from the point at which the boundary layer develops. Here, focusing attention on the mid-point of the bottom wall, we note that R_x has the meaning of the Reynolds number based on the radius of the convection cell, and is therefore equal to $(\Gamma/2)R_H \approx 0.1\Gamma Pr^{-0.7}Ra^{0.49}$ because of (D 2). Using (7.1), we can now obtain δ_1/λ.

To obtain δ_2/λ, the following additional facts are needed. In turbulent boundary layers, the vertical distance at which the Reynolds shear stress is equal to the viscous stress is about $12\nu/u_\tau$, where the so-called friction velocity u_τ is given by the definition that $\rho u_\tau^2 = \tau$. From the analysis of the data of Wieghardt & Tillmann (1951), we have

$$R_\tau \equiv u_\tau\delta/\nu = R_x^{0.709}. \tag{F 4}$$

A little algebra puts the rest of the details in place as above.

REFERENCES

Ahlers, G. 2001 Effect of sidewall conductance on heat-transport measurements for turbulent Rayleigh-Benard convection. *Phys. Rev.* E **63**, art. 015303.

Ahlers, G. & Xu, X. C. 2001 Prandtl-number dependence of heat transport in turbulent Rayleigh-Benard convection. *Phys. Rev. Lett.* **86**, 3320–3323.

Ashkenazi, S. & Steinberg, V. 1999 High Rayleigh number turbulent convection in a gas near the gas-liquid critical point. *Phys. Rev. Lett.* **83**, 3641–3644.

Busse, F. H. 1967 The stability of finite amplitude cellular convection and its relation to an extremum principle. *J. Fluid Mech.* **30**, 625–649.

Busse, F. H. 1978 Non-linear properties of thermal convection *Rep. Prog. Phys.* **41**, 1929–1967.

Castaing, B., Gunaratne, G., Heslot, F., Kadanoff, L., Libchaber, A., Thomae, S., Wu, X. Z., Zaleski, A. & Zanetti, G. 1989 Scaling of hard thermal turbulence in Rayleigh–Bénard convection. *J. Fluid Mech.* **204**, 1–30.

Chavanne, X. 1997 Etude du régime turbulent en convection de Rayleigh-Bénard dans l'hélium liquide ou gazeux autour de 5 K. PhD thesis, Université Joseph Fourier, Grenoble, France.

Chavanne, X., Chilla, F., Castaing, B., Hebral, B., Chabaud, B. & Chaussy, J. 1997 Observations of the ultimate regime in Rayleigh-Bénard convection. *Phys. Rev. Lett.* **79**, 3648–3651.

Chavanne, X., Chilla, F., Chabaud, B., Castaing, B. & Hebral, B. 2001 Turbulent Rayleigh-Bénard convection in gaseous and liquid He. *Phys. Fluids* **13**, 1300–1320 (referred to herein as II).

Childs, G. E., Ericks, L. J. & Powell, R. L. 1973 Thermal conductivity of solids at room temperature and below. *NBS Monograph* 131, pp. 533–574.

Cioni, S., Ciliberto, S. & Sommeria, J. 1997 Strongly turbulent Rayleigh-Bénard convection in mercury: comparison with results at moderate Prandtl number. *J. Fluid Mech.* **335**, 111–140.

Creveling, H. F., De Paz, J. F., Baladi, J. Y. & Schoenhals, R. J. 1975 Stability characteristics of a single-phase free convection loop. *J. Fluid Mech.* **67**, 65–84.

Goldstein, R. J., Chiang, H. D. & See, D. L. 1990 High-Rayleigh-number convection in a horizontal enclosure. *J. Fluid Mech.* **213**, 111–126.

Grossmann, S. & Lohse, D. 2000 Scaling in thermal convection: a unifying theory. *J. Fluid Mech.* **407**, 27–56.

Grossmann, S. & Lohse, D. 2001 Thermal convection for large Prandtl numbers. *Phys. Rev. Lett.* **86**, 3316–3319.

Grossmann, S. & Lohse, D. 2002 Prandtl and Rayleigh number dependence of the Reynolds number in turbulent thermal convection. *Phys. Rev.* E **66**, art. 016305.

Howard, L. N. 1966 Convection at high Rayleigh number. *Proc. Eleventh Intl Congr. on Applied Mechanics* (ed. H. Görtler), pp. 1109–1115. Springer.

Jensen, J. E., Stewart, R. B., Tuttle, W. A., Brechna, H. & Prodell, A. G. 1980 *Brookhaven National Laboratory Report* BNL 10200-R, vol. 1, *Selected Cryogenic Data Notebook*. Associated Universities, Inc. New York.

Kerr, R. M. 1996 Rayleigh number scaling in numerical convection. *J. Fluid Mech.* **310**, 139–179.

Kerr, R. M. & Herring, J. R. 2000 Prandtl number dependence of Nusselt number in direct numerical simulations. *J. Fluid Mech.* **419**, 325–344.

Kraichnan, R. H. 1962 Turbulent thermal convection at arbitrary Prandtl number. *Phys. Fluids* **5**, 1374–1389.

Krishnamurti, R. & Howard, L. N. 1981 Large-scale flow generation in turbulent convection. *Proc. Natl Acad. Sci.* **78**, 1981–1985.

Lam, S., Shang, X.-D., Zhou, S.-Q. & Xia, K.-Q. 2002 Prandtl number dependence of the viscous boundary layer and the Reynolds numbers in Rayleigh-Bénard convection. Submitted to *Phys. Rev.* E

Malkus, W. V. R. 2001 Borders of disorder. *Stud. Appl. Maths* **107**, 325–336.

Narasimha, R. & Sreenivasan, K. R. 1979 Relaminarization of fluid flows. *Adv. Appl. Mech.* **19**, 221–309.

Niemela, J. J., Skrbek, L., Sreenivasan, K. R. & Donnelly, R. J. 2000 Turbulent convection at very high Rayleigh numbers. *Nature* **404**, 837–840 (referred to herein as I).

Niemela, J. J., Skrbek, L., Sreenivasan, K. R. & Donnelly, R. J. 2001*a* The wind in confined thermal convection. *J. Fluid Mech.* **449**, 169–178.

Niemela, J. J., Skrbek, L., Sreenivasan, K. R. & Donnelly, R. J. 2001*b* Comments on high Rayleigh number convection. In *Proc. 1999 IUTAM Sympo. on Geometry and Structure of Turbulence* (ed. T. Kambe, T. Nakano & T. Miyauchi), pp. 269–277. Kluwer.

Palm, E. 1960 On the tendency towards hexagonal cells in steady convection. *J. Fluid Mech.* **8**, 183–192.

Preston, J. H. 1958 The minimum Reynolds number for a turbulent boundary layer and the selection of a transition device. *J. Fluid Mech.* **3**, 373–384.

Qiu, X.-L. & Tong, P. 2001 Large-scale structures in turbulent thermal convection. *Phys. Rev.* E **64**, art. 036304.

Roche, P. E. 2001 Convection thermique turbulente en cellule de Rayleigh-Bènard cryogénique. PhD Thesis, Centre de Recherche sur les Trés Basses Températures Laboratoire CNRS associé á Université Joseph Fourier.

Roche, P. E., Castaing, B., Chabaud, B. & Hebral, B. 2002 Prandtl number and Rayleigh-number dependences in Rayleigh Bénard convection. *Europhys. Lett.* **58**, 693–698.

Roche, P. E., Castaing, B., Chabaud, B., Hebral, B. & Sommeria, J. 2001 Sidewall effects in Rayleigh-Bénard convection. *Eur. Phys. J.* **24**, 405–408.

Sano, M., Wu, X.-Z. & Libchaber, A. 1989 Turbulence is helium gas free convection. *Phys. Rev.* A **40**, 6421–6430.

Shraiman, B. I. & Siggia, E. D. 1994 Heat transport in high-Rayleigh-number convection. *Phys. Rev.* E **26**, 137–168.

Sparrow, E. M., Husar, R. B. & Goldstein, R. J. 1970 Observations and other characteristics of thermals. *J. Fluid Mech.* **41**, 793–800.

Sreenivasan, K. R. 2000 Corrections due to sidewall conduction in turbulent convection problems. Unpublished report.

Sreenivasan, K. R., Bershadskii, A. & Niemela, J. J. 2002 Mean wind and its reversal in thermal convection. *Phys. Rev.* E **65**, art. 056306.

Sreenivasan, K. R. & Donnelly, R. J. 2001 Role of cryogenic helium in classical fluid dynamics: basic research and model testing. *Adv. Appl. Mech.* **37**, 239–276.

Takeshita, T., Segawa, T., Glazier, J. A. & Sano, M. 1996 Thermal turbulence in mercury. *Phys. Rev. Lett.* **76**, 1465–1468.

Townsend, A. A. 1959 Temperature fluctuations over an heated surface *J. Fluid Mech.* **5**, 209–241.

Tritton, D. J. 1988 *Physical Fluid Dynamics.* Clarendon.

Verzicco, R. 2002 Sidewall finite conductivity effects in confined turbulent thermal convection. *J. Fluid Mech.* **473**, 201–210.

Verzicco, R. & Camussi, R. 1999 Prandtl number effects in convective turbulence. *J. Fluid Mech.* **383**, 55–73.

Verzicco, R. & Camussi, R. 2003 Numerical experiments on strongly turbulent thermal convection in a slender cylindrical cell. *J. Fluid Mech.* **477**, 19–49.

Wieghardt, K. & Tillmann, W. 1951 On the turbulent friction layer for rising pressure. *NACA Tech. Memo.* 1314.

Wu, X.-Z. 1991 Along the road to developed turbulence: free thermal convection in low temperature helium. PhD thesis, University of Chicago, IL.

Wu, X.-Z. & Libchaber, A. 1991 Non-Boussinesq effects in free thermal convection. *Phys. Rev.* A **43**, 2833–2839.

Xin, Y.-B., Xia, K.-Q. & Tong, P. 1996 Measured velocity boundary layers in turbulent convection. *Phys. Rev. Lett.* **77**, 1266–1269.

Xu, X., Bajaj, K. M. S. & Ahlers, G. 2000 Heat transport in turbulent Rayleigh-Bénard convection. *Phys. Rev. Lett.* **84**, 4357–4360.